

Accepted Manuscript

Facile synthesis of Mn_3O_4 /reduced graphene oxide nanocomposites with enhanced capacitive performance

Yuqin Wang, Zhenyuan Ji, Xiaoping Shen, Keqiang Xu, Aihua Yuan



PII: S0925-8388(16)31479-7

DOI: [10.1016/j.jallcom.2016.05.146](https://doi.org/10.1016/j.jallcom.2016.05.146)

Reference: JALCOM 37666

To appear in: *Journal of Alloys and Compounds*

Received Date: 9 April 2016

Revised Date: 13 May 2016

Accepted Date: 14 May 2016

Please cite this article as: Y. Wang, Z. Ji, X. Shen, K. Xu, A. Yuan, Facile synthesis of Mn_3O_4 /reduced graphene oxide nanocomposites with enhanced capacitive performance, *Journal of Alloys and Compounds* (2016), doi: 10.1016/j.jallcom.2016.05.146.

This is a PDF file of an unedited manuscript that has been accepted for publication. As a service to our customers we are providing this early version of the manuscript. The manuscript will undergo copyediting, typesetting, and review of the resulting proof before it is published in its final form. Please note that during the production process errors may be discovered which could affect the content, and all legal disclaimers that apply to the journal pertain.

**Facile synthesis of Mn₃O₄/reduced graphene oxide
nanocomposites with enhanced capacitive performance**

Yuqin Wang,^a Zhenyuan Ji,^a Xiaoping Shen,^a * Keqiang Xu,^a and Aihua Yuan^b

^a *School of Chemistry and Chemical Engineering, Jiangsu University, Zhenjiang
212013, P. R. China*

^b *School of Environmental and Chemical Engineering, Jiangsu University of Science
and Technology, Zhenjiang 212003, P. R. China*

* Corresponding author. Tel.: +86 511 84401889; Fax: +86 511 88791800

E-mail address: xiaopingshen@163.com (Xiaoping Shen)

Abstract: In this study, a facile refluxing approach has been developed to load Mn_3O_4 nanocrystals onto reduced graphene oxide (RGO) sheets. The microstructure and morphology of the resulting $\text{Mn}_3\text{O}_4/\text{RGO}$ nanocomposites were systematically investigated by X-ray diffraction (XRD), Raman spectroscopy and transmission electron microscopy (TEM). The results reveal that Mn_3O_4 nanocrystals with particle size of several nanometers were uniformly dispersed on the surface of RGO sheets. The electrochemical properties of the resulting $\text{Mn}_3\text{O}_4/\text{RGO}$ nanocomposites were investigated by using them as electrode materials for a supercapacitor. It is found that the $\text{Mn}_3\text{O}_4/\text{RGO}$ nanocomposites exhibit enhanced specific capacitance and long-term stability. The enhanced capacitive performance can be attributed to the synergistic effect among Mn_3O_4 and RGO. The facile synthesis and the enhanced capacitive performance demonstrate the promising application of the $\text{Mn}_3\text{O}_4/\text{RGO}$ nanocomposites as supercapacitor electrode materials.

Keywords: Graphene; Hausmannite; Nanocomposite; Synthesis; Supercapacitor.

1. Introduction

With the increasing demand for clean and sustainable energy, high-efficient energy storage devices have attracted significant attention [1,2]. Supercapacitors represent a new type of energy storage devices that have the advantages of high power density, long service life, wide working temperature range, and environmental friendliness [3-6]. It is well accepted that the electrical energy storage of supercapacitors greatly depends on the used electrode materials. At present, the most extensively investigated electrode materials are carbonaceous materials, metal oxides and conductive polymers [7-9]. Among them, metal oxides with variable valence conduct fast and reversible faradaic reactions at the interface of the electrode and the electrolyte, which contribute to better supercapacitive properties [10]. Due to its notable specific capacitances, RuO_2 has been widely exploited in electrochemical capacitor electrodes [11]. Nevertheless, the commercialization is not promising because of its high cost and toxic effects [12,13]. Therefore, great efforts have been devoted toward replacing RuO_2 with inexpensive transition-metal oxides to meet the increasing demand for renewable energy storage devices.

Due to its high abundance, environmental compatibility and wide potential windows, hausmannite (Mn_3O_4) is a potentially interesting electrode material for supercapacitors and has drawn particularly research attention [14-16]. Unfortunately,

Mn_3O_4 often suffer from small specific surface area and intrinsically poor electrical conductivity, which severely affects the performance of supercapacitors [17]. To address these shortcomings, a common strategy is to combine Mn_3O_4 into nanocomposites with carbonaceous materials, which is both lightweight and electronically conducting [18]. Graphene, which consists of a well-defined two-dimensional honeycomb-like network of carbon atoms, has been widely used as conducting additive for nanocomposite materials due to its excellent electronic conductivity, high mechanical strength and large theoretical surface area [19-21]. The incorporation of graphene sheets with Mn_3O_4 can potentially construct conductivity network and effectively buffer the volume change effect [22,23]. To achieve a better electrode performance, it is expected that Mn_3O_4 nanoparticles with well-controlled size are uniformly anchored on the surface of graphene sheets [24]. Although some attempts have been made in the synthesis of Mn_3O_4 /graphene nanocomposites by different synthetic approaches, these preparation methods of Mn_3O_4 /graphene nanocomposites usually involved relatively complicated synthetic processes. Moreover, severe agglomeration of Mn_3O_4 nanoparticles often occurred in these nanocomposites. Therefore, a facile and effective method is still highly desirable for the synthesis of Mn_3O_4 nanoparticles with good controllability and high dispersivity on graphene sheets.

In this work, we report the fabrication of Mn_3O_4 /reduced graphene oxide (RGO) nanocomposites through a facile one-pot refluxing approach. GO was converted to RGO with triethylene glycol as the reducing agent, and no hazardous or toxic reductants were used. Well-dispersed Mn_3O_4 nanocrystals with particle size of several nanometer were uniformly attached on the surface of RGO sheets. The as-obtained Mn_3O_4 /RGO nanocomposites as electrode materials for supercapacitor exhibited enhanced capacitive performance, which makes it a promising candidate in supercapacitor electrodes.

2. Experimental

2.1. Chemicals

Natural flake graphite (45 μm , 99.95%) was obtained from Aladdin Industrial Corporation (Shanghai, China). All of the other reagents employed in this study are commercially available analytical-grade and used as received without further purification.

2.2. Preparation of Mn_3O_4 /RGO nanocomposites

Graphite oxide was prepared from the natural flake graphite according to a modified Hummers method [25,26]. In a typical procedure to synthesize the

Mn₃O₄/RGO nanocomposites, 25 mg of graphite oxide were dispersed in 50 mL of triethylene glycol by ultrasonication to form a homogeneous dispersion. A certain amount of manganese acetylacetonate (Mn(acac)₃) was then added and stirred continuously for 15 min at room temperature. The resulting mixture was then transferred into a 100 mL round-bottomed flask and heated at 250 °C under magnetic stirring for 1 h. After naturally cooled to room temperature, the solid products were isolated by centrifugation, washed thoroughly with water and ethanol, and finally dried in a vacuum oven at 50 °C for 12 h. For comparison, three Mn₃O₄/RGO samples with different Mn₃O₄ loading amounts were fabricated by changing the used amount of Mn(acac)₃. The products were designated as Mn₃O₄/RGO-0.25, Mn₃O₄/RGO-0.35 and Mn₃O₄/RGO-0.45 for the feeding amount of 0.25, 0.35 and 0.45 g of Mn(acac)₃, respectively.

2.3 Instrumentation and measurements

The crystalline phases of Mn₃O₄/RGO nanocomposites were analyzed by powder X-ray diffraction (XRD) on a Bruker D8 Advance diffractometer with Cu K_α radiation ($\lambda = 1.5406 \text{ \AA}$). The morphology and size of the products were examined by transmission electron microscopy (TEM) and high resolution TEM (HRTEM, JEOL JEM-2100). Raman scattering was collected at room temperature using a DXR Raman spectrometer with 532 nm laser source from an Ar⁺ laser.

2.4 Electrochemical measurements

Electrochemical measurements were performed on a beaker-type three-electrode setup using a CHI 760D electrochemical analyzer (Chen Hua Instruments, Shanghai, China) at room temperature. A platinum foil and a saturated calomel electrode (SCE) were used as counter electrode and reference electrode, respectively. The working electrodes were fabricated by mixing 80 wt% electroactive materials ($\text{Mn}_3\text{O}_4/\text{RGO}$), 10 wt% acetylene black and 10 wt% poly (vinylidene fluoride) (PVDF) binder in *N*-methyl-2-pyrrolidone solvent, and then the mixture was stirred for about 24 h to form a homogeneous slurry. After that, the slurry was pasted onto a nickel foam (surface area 1 cm^2), and then the nickel foam was placed into a vacuum oven at $60 \text{ }^\circ\text{C}$ for 48 h. The electrodes loaded with the active material were then pressed at 10 MPa. The mass of the $\text{Mn}_3\text{O}_4/\text{RGO}$ nanocomposites in the working electrodes was about 1.5 mg. Cyclic voltammetry (CV) and chronopotentiometry techniques were carried out to evaluate the electrochemical properties of the obtained products in 1 M Na_2SO_4 aqueous solution at room temperature. The specific capacitances of the nanocomposites were calculated according to the following equation [27]:

$$C_s = I\Delta t / (m\Delta V) \quad (1)$$

where C_s (F/g) is the specific capacitance of the electrodes, I (mA) is the charge-discharge current, Δt (s) is the discharge time, ΔV (V) represents the potential drop during discharge, and m (mg) is the mass of the electroactive material ($\text{Mn}_3\text{O}_4/\text{RGO}$) within the electrode.

3. Results and Discussion

In this work, we present a facile refluxing approach for the fabrication of $\text{Mn}_3\text{O}_4/\text{RGO}$ nanocomposites (Fig. 1). During the synthesis process, negatively charged GO nanosheets were firstly prepared by ultrasonication in triethylene glycol. When $\text{Mn}(\text{acac})_3$ was added into the GO solution, Mn^{3+} ions were absorbed onto the basal planes of GO sheets through electrostatic interaction. After being heated at 250 °C for 1 h, Mn_3O_4 nanocrystals was in-situ formed on GO sheets. At the same time, GO was reduced into RGO by using triethylene glycol as reducing agent. Finally, $\text{Mn}_3\text{O}_4/\text{RGO}$ nanocomposites with Mn_3O_4 nanocrystals uniformly anchored on RGO sheets were successfully obtained. XRD patterns of the as-synthesized graphite oxide and $\text{Mn}_3\text{O}_4/\text{RGO}-0.35$ nanocomposites are shown in Fig. 2. In the case of graphite oxide, the obvious diffraction peak located at around 11° corresponds to the (001) diffraction of graphite oxide [28]. For $\text{Mn}_3\text{O}_4/\text{RGO}-0.35$ nanocomposites, the

disappearance of the (001) peak of graphite oxide and appearance of the broad (002) diffraction peak arising from the short-range ordered stacking of graphene nanosheets at 2θ of about 25° demonstrate that graphite oxide has been well flaked to GO and successfully reduced into RGO during the synthesis process. All other diffraction peaks can be well indexed to tetragonal structure of Mn_3O_4 (JCPDS No. 24-0734), demonstrating the formation of Mn_3O_4 nanocrystals.

Raman spectroscopy is an effective method to characterize the disorder and defects of graphene based materials. Fig. 3 shows the typical Raman spectra of graphite oxide and $\text{Mn}_3\text{O}_4/\text{RGO}-0.35$ nanocomposites. Two prominent characteristic peaks attributing to the well-documented G and D bands can be observed in both the samples. D peak represents the structure defects and the disorder, while G peak derives from the E_{2g} vibration mode of C sp^2 atoms [29,30]. The D peak and G peak integrated intensity ratio (I_D/I_G) can be used to evaluate the defects and the degree of disorder in carbon structure [31,32]. In this experiment, the ratios of I_D/I_G for graphite oxide and $\text{Mn}_3\text{O}_4/\text{RGO}-0.35$ nanocomposites are 1.52 and 1.85, respectively. The increase in I_D/I_G value for $\text{Mn}_3\text{O}_4/\text{RGO}$ implies that more disordered carbon structure and defects were brought after the exfoliation of graphite oxide and introduction of Mn_3O_4 nanocrystals on the RGO nanosheets [33]. In addition, $\text{Mn}_3\text{O}_4/\text{RGO}-0.35$ presents one diagnostic Raman scattering band of Mn_3O_4 at about 651 cm^{-1} ,

evidencing the presence of Mn_3O_4 in the nanocomposites [34]. The morphology, particle size and crystallinity of the $\text{Mn}_3\text{O}_4/\text{RGO}$ nanocomposites have been investigated using TEM images. Fig. 4 shows representative TEM and HRTEM images of $\text{Mn}_3\text{O}_4/\text{RGO}$ -0.35 nanocomposites. It is found that the $\text{Mn}_3\text{O}_4/\text{RGO}$ has sheet-like morphology, and the RGO nanosheets are covered by a uniform layer of Mn_3O_4 nanocrystals. The high uniformity of the hybrid structure suggests a good combination between the nanoparticles and RGO. This demonstrates that our one-step refluxing approach is efficient to synthesize $\text{Mn}_3\text{O}_4/\text{RGO}$ nanocomposites. From the HRTEM image shown in Fig. 4b, the average size of the Mn_3O_4 nanocrystals is determined to be about 3 nm.

The electrochemical performance of the as-prepared $\text{Mn}_3\text{O}_4/\text{RGO}$ nanocomposites was first evaluated by means of cycle voltammetry in a three electrode system with 1 M Na_2SO_4 electrolyte at a potential range from 0 to 1.0 V. As shown in Fig. 5a, the RGO and $\text{Mn}_3\text{O}_4/\text{RGO}$ nanocomposites have nearly rectangle-shaped and symmetric CV curves without any redox peak currents at scan rate of 50 mV/s, suggesting the ideal capacitive behaviours [26]. Obviously, there is a remarkable difference in the CV loop areas observed among RGO and $\text{Mn}_3\text{O}_4/\text{RGO}$ electrodes. Since the specific capacitance is proportional to the CV loop area, it is evident from the CV curves that $\text{Mn}_3\text{O}_4/\text{RGO}$ electrodes have greater specific

capacitance in compared with RGO, and $\text{Mn}_3\text{O}_4/\text{RGO}-0.35$ electrode exhibits the highest specific capacitance. Fig. 5b shows the specific capacitance of $\text{Mn}_3\text{O}_4/\text{RGO}-0.35$ nanocomposite as a function of the scan rate. It can be seen that all the curves are close to a rectangular shape and exhibit mirror image characteristics which indicate that the Faraday redox reactions are electrochemically reversible. The CV current response of $\text{Mn}_3\text{O}_4/\text{RGO}-0.35$ increases gradually with the increase of scan rate and no significant change in the shape of CV curve even at high scan rate, indicating an excellent capacitance behavior and the fast diffusion of electrolyte ions into the $\text{Mn}_3\text{O}_4/\text{RGO}-0.35$ nanocomposite electrode [35].

To further illustrate the electrochemical performance of the as-prepared electrodes, galvanostatic charge-discharge measurements were conducted in Na_2SO_4 solution at different current densities over the potential range of 0-1 V. Fig. 6a shows galvanostatic charge-discharge curves of the as-prepared RGO and $\text{Mn}_3\text{O}_4/\text{RGO}$ nanocomposites at 0.5 A/g. The charge/discharge time varies at a constant current density for RGO and $\text{Mn}_3\text{O}_4/\text{RGO}$ electrodes, suggesting different specific capacitances. The increase in the charging time represents the higher capacitance. Obviously, the $\text{Mn}_3\text{O}_4/\text{RGO}-0.35$ electrode shows a longest charge-discharge time in its curve, implying that it has a largest capacitance among all these materials, which is well consistent with the result obtained from CV curves. Fig. 6b displays the

charge-discharge curves of the $\text{Mn}_3\text{O}_4/\text{RGO}-0.35$ nanocomposites at various current densities. It can be seen that the discharge time gradually decreases with the increase of the current density from 0.5 to 5 A/g. Moreover, no obviously shape change can be observed among the nearly linear charge/discharge curves at different scan rates, indicating that the $\text{Mn}_3\text{O}_4/\text{RGO}-0.35$ nanocomposite possesses good reversibility and rate capability. The specific capacitance of electrodes at different current densities can be calculated according to the equation (1). As shown in Fig. 6c, the specific capacitances descend with the increasing current density. The higher specific capacitance at low current density is due to the sufficient transfer time for ions between the electrolyte and the electrode [36,37]. The specific capacitances of RGO and $\text{Mn}_3\text{O}_4/\text{RGO}$ nanocomposites increase in the following order: $\text{RGO} < \text{Mn}_3\text{O}_4/\text{RGO}-0.25 < \text{Mn}_3\text{O}_4/\text{RGO}-0.45 < \text{Mn}_3\text{O}_4/\text{RGO}-0.35$. The $\text{Mn}_3\text{O}_4/\text{RGO}-0.35$ electrodes show greatly enhanced specific capacitance compared to RGO and other $\text{Mn}_3\text{O}_4/\text{RGO}$ nanocomposites electrodes. The specific capacitances of $\text{Mn}_3\text{O}_4/\text{RGO}-0.35$ electrode at 0.5, 1, 2 and 5 A/g are 194.5, 180.8, 162.8 and 132.0 F/g, respectively, which is comparable to or higher than that of previously reported transition-metal-doped Mn_3O_4 and graphene/ Mn_3O_4 electrodes [38,39]. The increment in specific capacitance can be mainly attributed to the increased content of active component of Mn_3O_4 for capacitance generation. However, with the further increase

of Mn_3O_4 content in $\text{Mn}_3\text{O}_4/\text{RGO}$ nanocomposites, the content of graphene would accordingly decrease, which could cause the decrease of the electrical conductivity of $\text{Mn}_3\text{O}_4/\text{RGO}$ nanocomposites, and thereby lead to a decreased capacitance of $\text{Mn}_3\text{O}_4/\text{RGO}$ nanocomposites. Specific energy and specific power are key factors for evaluating the electrochemical properties of supercapacitors. The energy density and power density values are calculated according to galvanostatic charge-discharge curves from the following equations (equation (2) and (3)) [40,41]:

$$E = (C\Delta V^2)/7.2 \quad (2)$$

$$P = 3600 E/\Delta t \quad (3)$$

where E (W h/kg) is the average energy density, C (F/g) is the total specific capacitance, ΔV (V) is the potential window during discharge, P (W/kg) is the average power density, and Δt (s) represents the discharge time. Fig. 6d shows the Ragone plots for RGO and $\text{Mn}_3\text{O}_4/\text{RGO}$ nanocomposites electrodes. It can be observed that the $\text{Mn}_3\text{O}_4/\text{RGO}$ -0.35 electrode can achieve the highest energy density under the same power density among all these electrodes. The specific energy density of $\text{Mn}_3\text{O}_4/\text{RGO}$ -0.35 nanocomposites can reach to 27 W h/kg at a power density of 250 W/kg, and still remains 18.3 W h/kg at a high power density of 2500 W/kg, demonstrating promising application in supercapacitor electrode materials.

The cycle stability of supercapacitors is a crucial parameter for their practical applications. In this study, the cycling stability of $\text{Mn}_3\text{O}_4/\text{RGO}-0.35$ electrode was evaluated by repeating the charge-discharge measurements at a constant current density of 5 A/g. Fig. 7 shows specific capacitance values of the initial 1000 cycles as a function of cycle number. It can be seen that the specific capacitance value decreases gradually within the first 500 cycles and then remains almost constant in the residual cycles. The cycling stability of the $\text{Mn}_3\text{O}_4/\text{RGO}-0.35$ electrode is outstanding with 77% capacitance retention after 1000 continuous cycles.

4. Conclusions

In summary, $\text{Mn}_3\text{O}_4/\text{RGO}$ nanocomposites have been successfully prepared by a facile refluxing approach. Highly dispersed Mn_3O_4 nanocrystals with a size of several nanometer were in situ grown on the surface of RGO sheets with uniform particle distribution. The prepared $\text{Mn}_3\text{O}_4/\text{RGO}$ nanocomposites were used as electrode materials for supercapacitor. It is found that a suitable content of Mn_3O_4 in $\text{Mn}_3\text{O}_4/\text{RGO}$ nanocomposites is crucial to optimize the capacitive performance. $\text{Mn}_3\text{O}_4/\text{RGO}-0.35$ nanocomposite exhibits greatly enhanced capacitive performance and long-term stability. The facile synthesis and enhanced electrochemical property of

the $\text{Mn}_3\text{O}_4/\text{RGO}$ nanocomposites make them promising electrode materials for supercapacitor application.

Acknowledgements

The authors are grateful for financial support from the Natural Science Foundation of Jiangsu province (No. BK20150507), China Postdoctoral Science Foundation (2015M580393) and the Startup Fund for Distinguished Scholars of Jiangsu University (No. 15JDG023).

References

- [1] B. Dunn, H. Kamath, J.M. Tarascon, *Science* 334 (2011) 928-935.
- [2] H. Pang, Y.Z. Zhang, Z. Run, W.Y. Lai, W. Huang, *Nano Energy* 17 (2015) 339-347.
- [3] M. Vanithaa, Keerthi, P. Cao, N. Balasubramanian, *J. Alloy Compd.* 644 (2015) 534-544.
- [4] J. Yan, Q. Wang, T. Wei, Z.J. Fan, *Adv. Energy Mater.* 4 (2014) 157-164.
- [5] J. Pu, F.L. Cui, S.B. Chu, T.T. Wang, E.H. Sheng, Z.H. Wang, *ACS Sustainable Chem. Eng.* 2 (2014) 809-815.
- [6] B. Li, M.B. Zheng, H.G. Xue, H. Pang, *Inorg. Chem. Front.* 3 (2016) 175-202.
- [7] Y.W. Zhu, S. Murali, M.D. Stoller, K.J. Ganesh, W.W. Cai, P.J. Ferreira, A. Pirkle, R.M. Wallace, K.A. Cychoz, M. Thommes, D. Su, E.A. Stach, R.S. Ruoff, *Science* 332 (2011) 1537-1541.
- [8] L. Wang, Y.J. Hao, Y. Zhao, Q.Y. Lai, X.Y. Xu, *J. Solid State Chem.* 183 (2010) 2576-2581.
- [9] H.L. Wang, Q.L. Hao, X.J. Yan, L.D. Lu, X. Wang, *Electrochem. Commun.* 11 (2009) 1158-1161.
- [10] L. Yu, G.Q. Zhang, C.Z. Yuan, X.W. Lou, *Chem. Commun.* 49 (2013) 137-139.

- [11] Z. Wu, D. Wang, W. Ren, J. Zhao, G. Zhou, F. Li, H. Cheng, *Adv. Funct. Mater.* 20 (2010) 3595-3602.
- [12] X. Zhao, B.M. Sanchez, P. Dobson, P. Grant, *Nanoscale* 3 (2011) 839-855.
- [13] I.E. Rauda, V. Augustyn, B. Dunn, S.H. Tolbert, *Acc. Chem. Res.* 46 (2013) 1113-24.
- [14] B.G.S. Raj, A. M. Asiri, J.J. Wu, S. Anandan, *J. Alloy Compd.* 636 (2015) 234-240.
- [15] P. Li, C. Nan, Z. Wei, J. Lu, Q. Peng, Y. Li, *Chem. Mater.* 22 (2010) 4232-6.
- [16] F. Gao, J.Y. Qu, Z.B. Zhao, Q. Zhou, B.B. Li, J.S. Qiu, *Carbon* 80 (2014) 640-650.
- [17] W. Wei, X. Cui, W. Chen, D.G. Ivey, *Chem. Soc. Rev.* 40 (2011) 1697-721.
- [18] T. Chen, L. Dai, *J. Mater. Chem. A* 2 (2014) 10756-10775.
- [19] A. Majeed, W. Ullah, A.W. Anwar, F. Nasreen, A. Sharif, G. Mustafa, A. Khan, *J. Alloy Compd.* 671 (2016) 1-10.
- [20] S. Stankovich, D.A. Dikin, G.B. Dommett, K.M. Kohlhaas, E.J. Zimney, E.A. Stach, R.D. Piner, S.T. Nguyen, R.S. Ruoff, *Nature* 442 (2006) 282-286.
- [21] A.K. Geim, *Science* 324 (2009) 1530-1534.
- [22] Y. Huang, J.J. Liang, Y.S. Chen, *Small* 8 (2012) 1805-34.
- [23] L. Dong, Z.X. Chen, D. Yang, H.B. Lu, *Rsc Advances* 3 (2013) 21183-21191.

- [24] B.G.S. Raj, R.N.R. Ramprasad, A.M. Asiri, J.J. Wu, S. Anandan, *Electrochim. Acta* 156 (2015) 127-137.
- [25] W.S. Hummers, R.E. Offeman, *J. Am. Chem. Soc.* 80 (1958) 1339-1339.
- [26] Z.Y. Ji, X.P. Shen, M.Z. Li, H. Zhou, G.X. Zhu, K.M. Chen, *Nanotechnology* 24 (2013) 1-10.
- [27] H. Chen, L.F. Hu, M. Chen, Y. Yan, L.M. Wu, *Adv. Funct. Mater.* 24 (2014) 934-942.
- [28] T. Nakajima, A. Mabuchi, R. Hagiwara, *Carbon* 26 (1988) 357-361.
- [29] D. Graf, F. Molitor, K. Ensslin, C. Stampfer, A. Jungen, C. Hierold, L. Wirtz, *Nano Lett.* 7 (2007) 238-242.
- [30] B.B. Zhang, J.L. Song, G.Y. Yang, B.X. Han, *Chem. Sci.* 5 (2014) 4656-4660.
- [31] A.C. Ferrari, J.C. Meyer, V. Scardaci, C. Casiraghi, M. Lazzeri, F. Mauri, S. Piscanec, D. Jiang, K.S. Novoselov, S. Roth, A.K. Geim, *Phys. Rev. Lett.* 97 (2006) 13831-13840.
- [32] M.S. Dresselhaus, A. Jorio, M. Hofmann, G. Dresselhaus, R. Saito, *Nano Lett.* 10 (2010) 751-758.
- [33] Y.Y. Wen, H.M. Ding, Y.K. Shan, *Nanoscale* 3 (2011) 4411-4417.
- [34] J.Y. Qu, F. Gao, Q. Zhou, Z.Y. Wang, H. Hu, B.B. Li, W.B. Wan, X.Z. Wang, J.S. Qiu, *Nanoscale* 5 (2013) 2999-3005.

- [35] X. Fan, W. Peng, Y. Li, X. Li, S. Wang, G. Zhang, F. Zhang, *Adv. Mater.* 20 (2008) 4490-4493.
- [36] Z.J. Fan, J. Yan, T. Wei, L.J. Zhi, G.Q. Ning, T.Y. Li, F. Wei, *Adv. Funct. Mater.* 21 (2011) 2366-2375.
- [37] L.B. Ma, X.P. Shen, Z.Y. Ji, G.X. Zhu, H. Zhou, *Chem. Eng. J.* 252 (2014) 95-103.
- [38] R.T. Dong, Q.L. Ye, L.L. Kuang, X. Lu, Y. Zhang, X. Zhang, G.J. Tan, Y.X. Wen, F. Wang, *ACS Appl. Mater. Interfaces* 5 (2013) 9508-9516.
- [39] J.W. Lee, A.S. Hall, J.D. Kim, T.E. Mallouk, *Chem. Mater.* 24 (2012) 1158-1164.
- [40] H. Pang, Y.Z. Zhang, W.Y. Lai, Z. Hu, W. Huang, *Nano Energy* 15 (2015) 303-312.
- [41] Y.H. Xiao, Y.B. Cao, Y.Y. Gong, A.Q. Zhang, J.H. Zhao, S.M. Fang, D.Z. Jia, F. Li, *J. Power Sources* 246 (2014) 926-933.

Figure Captions

Fig. 1. A schematic diagram for the preparation of $\text{Mn}_3\text{O}_4/\text{RGO}$ nanocomposites.

Fig. 2. XRD patterns of graphite oxide and $\text{Mn}_3\text{O}_4/\text{RGO}$ nanocomposites.

Fig. 3. Raman spectra of graphite oxide and $\text{Mn}_3\text{O}_4/\text{RGO}$ -0.35 nanocomposites.

Fig. 4. (a) TEM and (b) HRTEM images of the $\text{Mn}_3\text{O}_4/\text{RGO}$ -0.35 nanocomposites.

Fig. 5. (a) CV curves of RGO and $\text{Mn}_3\text{O}_4/\text{RGO}$ nanocomposites at the scan rate of 50 mV/s; (b) CV curves of $\text{Mn}_3\text{O}_4/\text{RGO}$ -0.35 electrode at various scan rates.

Fig. 6. (a) Charge-discharge curves of RGO and $\text{Mn}_3\text{O}_4/\text{RGO}$ nanocomposites at the current density of 0.5 A/g; (b) charge-discharge curves of $\text{Mn}_3\text{O}_4/\text{RGO}$ -0.35 nanocomposites electrode at various current densities of 0.5, 1.0, 2.0 and 5.0 A/g; (c) the specific capacitance values of RGO and $\text{Mn}_3\text{O}_4/\text{RGO}$ nanocomposites electrodes as a function of current density; (d) Ragone plots of the estimated energy density and power density of RGO and $\text{Mn}_3\text{O}_4/\text{RGO}$ nanocomposites electrodes.

Fig. 7. The cycling performance of $\text{Mn}_3\text{O}_4/\text{RGO}$ -0.35 electrode at a constant current density of 5 A/g.

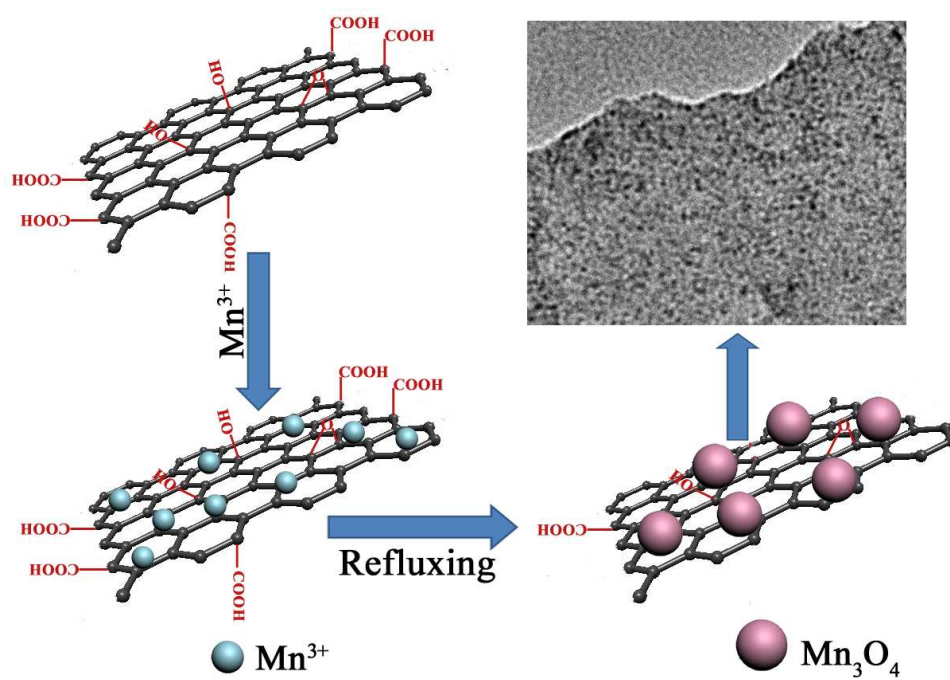


Figure 1

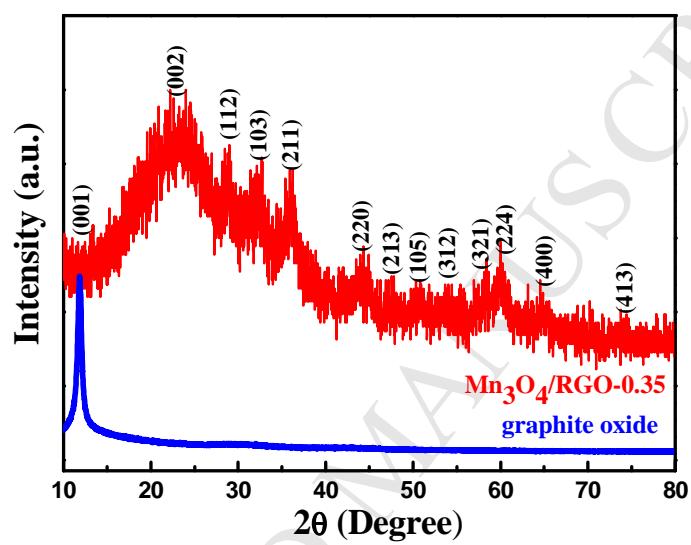


Figure 2

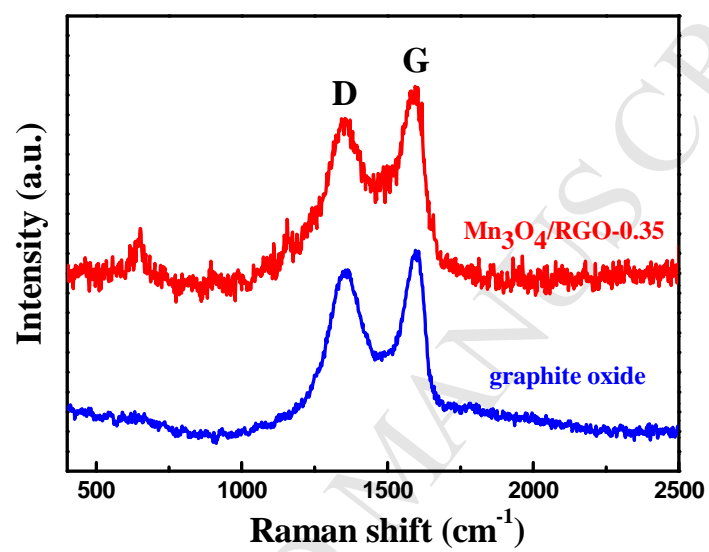


Figure 3

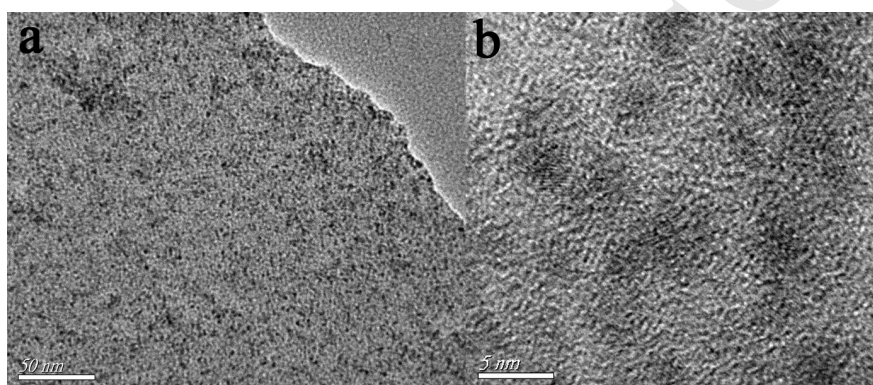


Figure 4

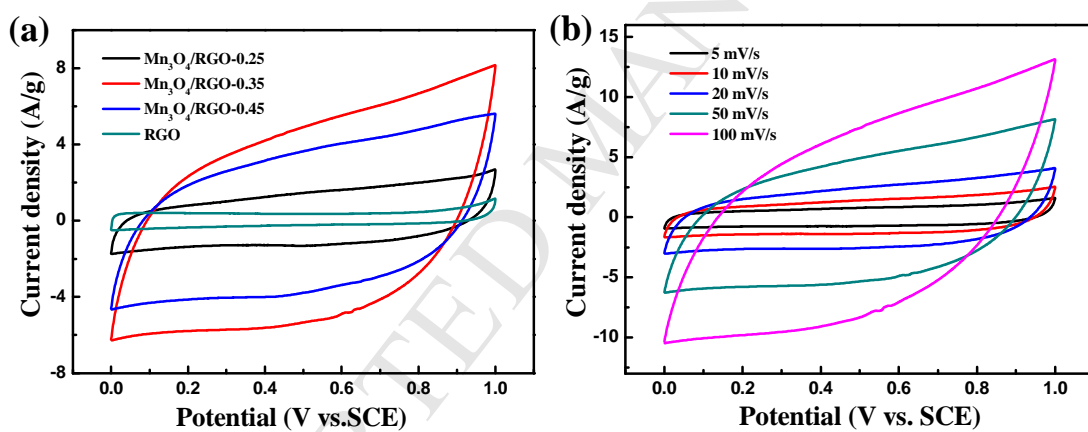


Figure 5

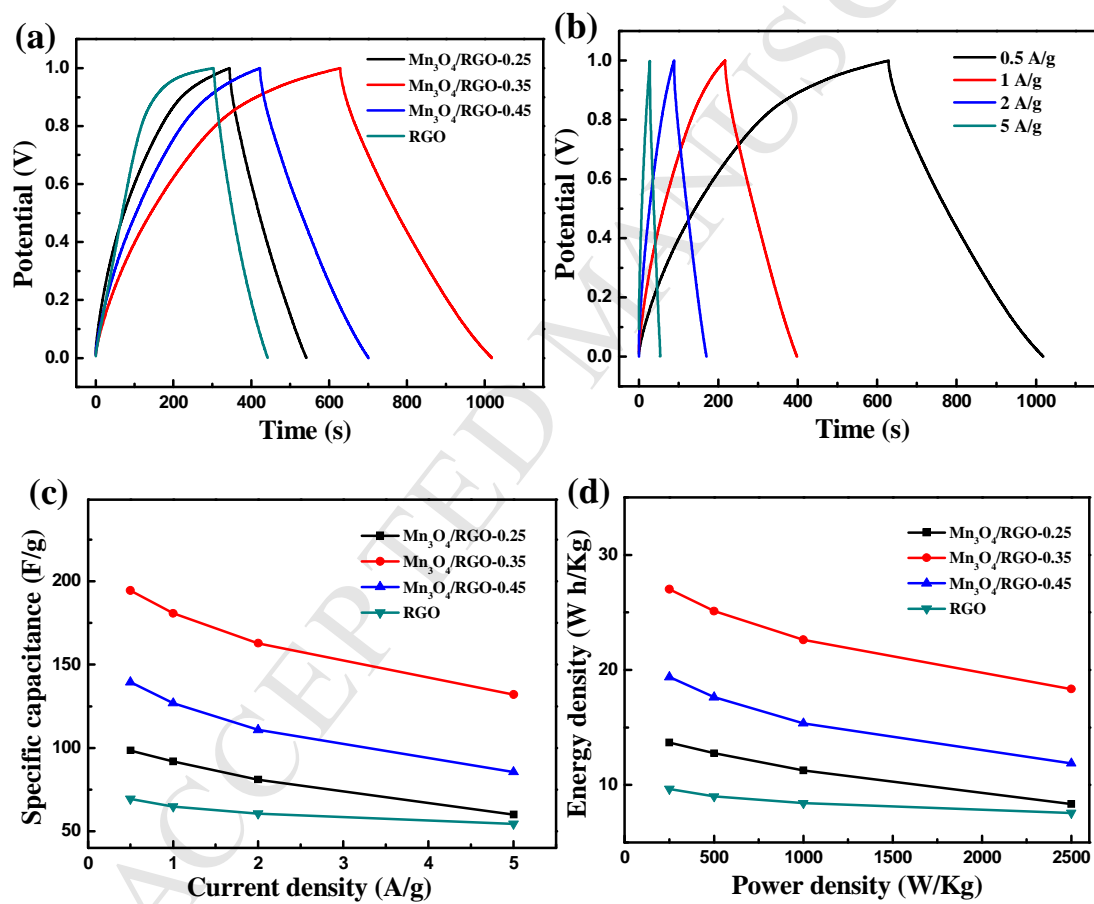


Figure 6

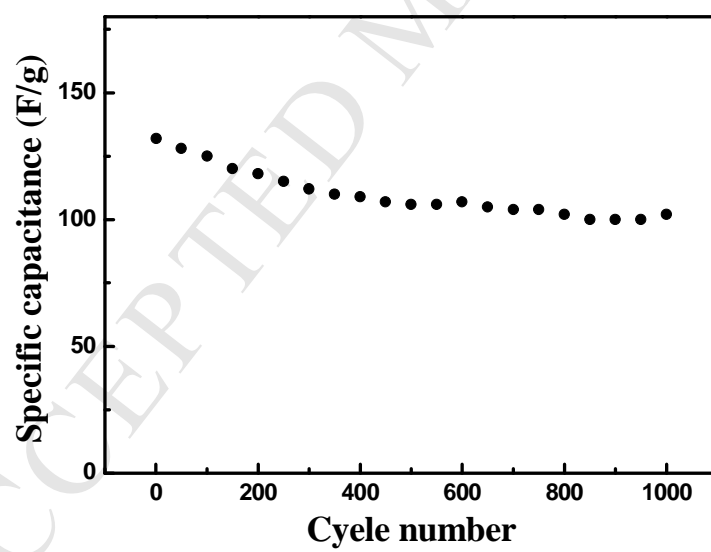


Figure 7

Mn₃O₄/RGO nanocomposites were synthesized through a facile one-step approach.

The capacitive performance of Mn₃O₄/RGO nanocomposites was significantly improved.

Possible mechanism for the enhanced capacitive performance was proposed.